Author(s): Wu, F. & Danneau, R. & Queipo, P. & Kauppinen, E. & Tsuneta, T. & Hakonen, Pertti J.

Title: Single-walled carbon nanotube weak links in Kondo regime with zero-field splitting

Year: 2009

Version: Final published version

Please cite the original version:

Wu, F. & Danneau, R. & Queipo, P. & Kauppinen, E. & Tsuneta, T. & Hakonen, Pertti J. 2009. Single-walled carbon nanotube weak links in Kondo regime with zero-field splitting. Physical Review B. Volume 79, Issue 7. 073404/1-4. ISSN 1098-0121 (printed). DOI: 10.1103/physrevb.79.073404

Single-walled carbon nanotube weak links in Kondo regime with zero-field splitting

F. Wu,[1] R. Danneau,[1,*] P. Queipo,[2] E. Kauppinen,[2] T. Tsuneta,[1] and P. J. Hakonen[1]
[1]*Low Temperature Laboratory, Helsinki University of Technology, P.O. Box 2200, 02015 HUT, Espoo, Finland*
[2]*Center for New Materials, Helsinki University of Technology, P.O. Box 1100, 02015 HUT, Espoo, Finland*
(Received 19 December 2008; published 13 February 2009)

We have investigated proximity-induced supercurrents in single-walled carbon nanotubes in the Kondo regime and compared them with supercurrents obtained on the same tube with Fabry-Pérot resonances. Our data display a wide distribution of Kondo temperatures $T_K=1-14$ K, and the measured critical current I_{CM} vs T_K displays two distinct branches; these branches, distinguished by zero-field splitting of the normal-state Kondo conductance peak, differ by an order of magnitude at large values of T_K. Evidence for renormalization of Andreev levels in Kondo regime is also found.

DOI: 10.1103/PhysRevB.79.073404 PACS number(s): 73.63.Fg

An odd unpaired electron in a strongly coupled quantum dot makes the dot to behave as a magnetic impurity screened by delocalized electrons. Such a Kondo impurity creates a peak in the density of states at the Fermi level, thereby leading to characteristic Kondo resonances with enhanced conductance around zero bias, which has been observed in various quantum dot systems during the recent years.[1–3] By studying low-bias transport and multiple Andreev reflections (MAR) in multiwalled carbon nanotubes (MWNTs) contacted by superconducting leads, it has been demonstrated that the Kondo resonances survive the superconductivity of the leads when the Kondo temperature T_K exceeds the superconducting gap Δ (Ref. 4); thus, intricate interplay between Kondo behavior and superconductivity can be studied in nanotube quantum dots.

In quantum dots made out of singlewalled carbon nanotubes (SWNTs), contacts play a crucial role in their transport properties: in the highly transparent regime, Fabry-Pérot (FP) interference patterns in the differential conductance can be observed,[5] whereas in the less transparent case, Coulomb-blockade peaks occur.[6] In the intermediate regime, zero-bias conductance peaks alternate with Coulomb-blockaded valleys, highlighting Kondo resonances below Kondo temperature T_K due to odd numbers of spin in the cotunneling process between the dot and the leads.[3]

Gate-controlled proximity-induced supercurrent has been reported both in SWNTs[7–12] and in MWNTs.[13,14] Reasonable agreement with resonant quantum dot weak link theories[15] has been reached in best of the samples (see, e.g., Ref. 9). In some of the experiments, Kondo-restored supercurrents were found[11,16] in the otherwise Coulomb-blockaded Josephson-junction case. In addition, when $T_K<\Delta$, π Josephson junctions have been observed.[10,11]

Here we report a study of gate-tunable proximity-induced supercurrents of an individual SWNT. We compare supercurrents in Fabry-Pérot and Kondo regimes at the same normal-state conductance and find smaller critical currents in the Kondo regime up to $T_K\sim 10\Delta$. In addition, we find that not just T_K but also the shape of the Kondo resonance conductance peak affects the magnitude of the supercurrent: resonances with zero-field splitting, which appear in about every second of our Kondo peaks, result in a smaller critical current than for the regular Kondo maxima.

Our nanotube samples were made using surface chemical-vapor deposition (CVD) growth with Fe catalyst directly on oxidized heavily doped SiO_2/Si wafer. The electrically conducting substrate works as a back gate, separated from the sample by 150 nm of SiO_2. A sample with $L=0.7$ μm length and $\phi=2$ nm diameter was located using an atomic force microscope and the contacts on the SWNT were made using standard e-beam overlay lithography. For the contacts, 10 nm of Ti was first evaporated, followed by 70 nm of Al, in order to facilitate proximity-induced superconductivity in Ti. Last, 5 nm of Ti was deposited to prevent the Al layer from oxidation. The width of the two contacts was 200 nm and the separation between the them was 0.3 μm.

The measurement leads were filtered using an *RC* filter with time constant of 10 μs at 1 K, followed by twisted pairs with tight, grounded electrical shields for filtering between the still and the mixing chamber, while the final section was provided by a 0.7-m-long Thermocoax cable on the sample holder. In the measurements, differential conductance $G_d=dI/dV$ was recorded using standard lock-in techniques. Voltage bias was imposed via a room-temperature voltage divider. The normal-state data were obtained by applying a magnetic field of $B\sim 70$ mT perpendicular to the nanotube. The superconducting gap of the device was taken from the 2Δ quasiparticle peak in voltage-biasing transport measurement, which gives $\Delta=125$ μeV, and gate capacitance $C_g=1.6$ aF was estimated from the measured gate period of 0.1 V.

The data presented in this Brief Report have been measured in several cool downs, thermal cycles, that have changed the contact conditions on our sample. In the first cool down, the sample showed a strongly asymmetric Fabry-Pérot pattern with one low-transmission (spin-degenerate) channel and another one with high transmission; the zero-bias conductance was limited to $2e^2/h$ as a consequence.[17] A scan of differential conductance $G_d(V_{ds},V_g)$ versus bias voltage V_{ds} and gate voltage V_g is shown in Fig. 1(a) at $B\sim 70$ mT. In the absence of magnetic field, a gate-voltage-dependent supercurrent is observed in the SWNT. The measured critical supercurrent I_{CM} varies periodically with the gate voltage V_g, reaching a maximum of 4.8 nA at zero-bias normal-state conductance $G_N=G_d|_{V_{ds}=0}=2.03e^2/h$. The $I_{CM}R_N$ product is V_g dependent and it changes in a similar fashion as I_{CM} and the inverse of the normal-state resistance G_N. This result is similar to what has been observed in a

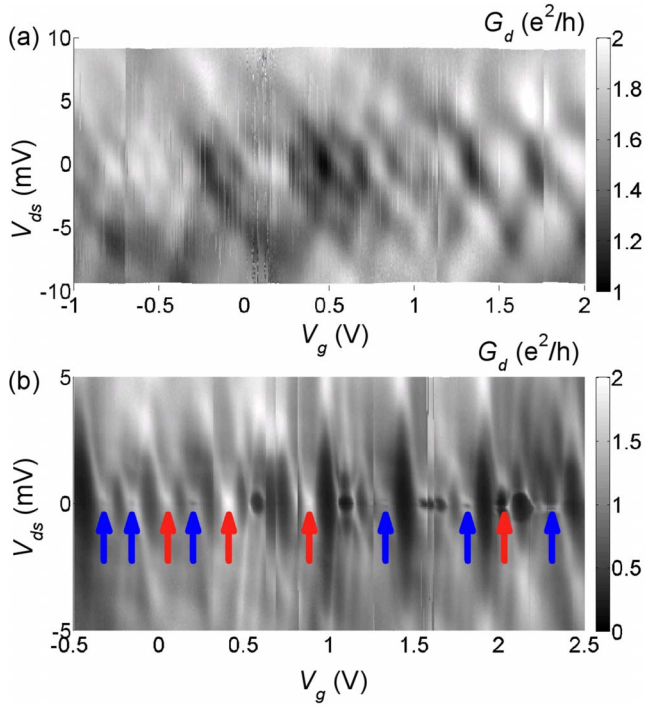

FIG. 1. (Color online) Normal-state differential conductance G_d on the plane spanned by bias voltage V_{ds} and gate voltage V_g in (a) Fabry-Pérot regime and (b) Kondo regime both at $T=30$ mK. Normal states were achieved in all the cases with a magnetic field $B=70$ mT. Red (light gray) and blue (dark gray) arrows in (b) refer to two types of resonance peaks, which have one magnitude difference in I_{CM} with similar Kondo temperature T_K. See text for more details.

superconducting SWNT in Fabry-Pérot regime.[9]

After a few thermal cycles, the transport of SWNT changed from Fabry-Pérot into Kondo type of behavior as seen in Fig. 1(b). The G_d map displays a series of Coulomb-blockade diamonds (even number of electrons) alternating with Kondo ridges, marked by the arrows (odd number of electrons). The Kondo ridges are rather wide and the Kondo temperatures, which are deduced from the half-width at half maximum of the resonant conductance peaks versus bias voltage $G_d(V_{ds})$ (see below) range over $T_K=1-14$ K. We find that both the critical current and zero-bias conductance are smaller compared with Fabry-Pérot regime, even in the Kondo resonances with the highest T_K.

The superconducting state IV curves in both Fabry-Pérot and Kondo regimes are shown in Fig. 2. As the sample is voltage-biased, negative differential resistance (NDR) is observable in Fabry-Pérot regime. However, in Kondo regime, NDR occurs only at small measured critical current I_{CM} and it disappears around the maximum of the Kondo resonance peak where I_{CM} is large. We note that zero-bias resistance and the IV curves evolve smoothly with V_g around the Kondo resonance without any sudden jumps, and that $T_K > \Delta$ so that there is no $0-\pi$ phase transition observed.[11,18] We ascribe the disappearance of NDR to the presence of large MAR-induced subgap current, which is stronger with respect to the supercurrent in the Kondo regime than in the FP case.[19]

The nanotube together with superconducting leads can be considered as a resonant-level quantum dot, and thus the two-barrier Breit-Wigner model is applicable to model the behavior.[15] In our case, the measured I_{CM} is nearly 1 order of magnitude smaller than the theoretical prediction $I_0=e\Delta/\hbar \approx 30$ nA with one resonant spin-degenerate level.[20] Taking into account the phase diffusion in an underdamped voltage-biased Josephson junction,[21] the measured $I_{\mathrm{CM}} \propto E_J^2 \propto I_C^2$. With the Breit-Wigner model for wide resonance limit $h\Gamma \gg \Delta$ and transmission probability α_{BW}, we have $I_C=I_0[1-(1-\alpha_{\mathrm{BW}})^{1/2}]$ so the $I_{\mathrm{CM}}-G_N$ relation can be written as

$$I_{\mathrm{CM}} = I_{0M}\left[1-\left(1-\frac{1}{2}g_n\right)^{1/2}\right]^2, \tag{1}$$

where I_{0M} denotes the maximum measurable critical current when the scaled conductance $g_n=G_N/(e^2/h)\to 2$. This equation is written for one spin-degenerate channel (the Kondo case) where the transmission coefficient is obtained from $\frac{1}{2}g_n$, and the prefactor depends on T_K; in our case it also applies approximately to the asymmetric FP conduction as one of the spin-degenerate transmission channels is greatly suppressed.[17] The fit of Eq. (1) to our data is displayed in

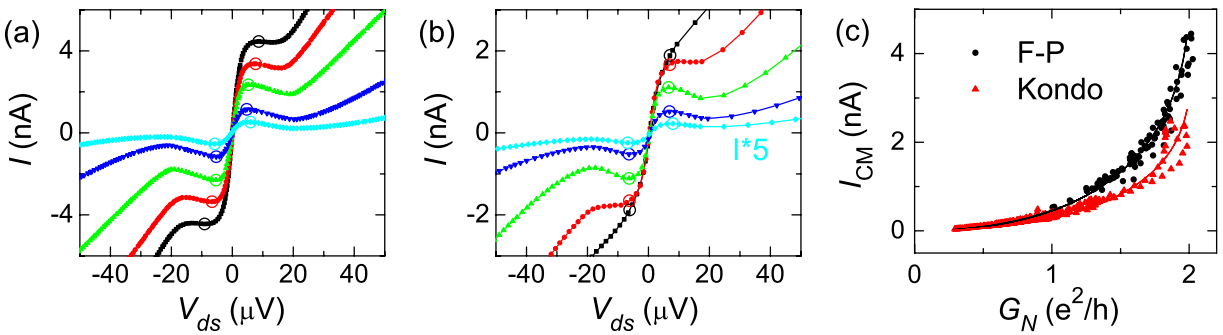

FIG. 2. (Color online) Superconducting I-V curves at a few gate voltage values in (a) Fabry-Pérot regime and (b) Kondo regime. The circles on each I-V curve show how the measured critical current I_{CM} was determined (Ref. 22). I_{CM} versus zero-bias normal-state conductance G_N, measured for a resonance with $T_K=14$ K, is displayed in (c) where the black dots and red (light gray) triangles refer to Fabry-Pérot (several resonances) and Kondo data, respectively. Data in (a) were measured in the same cool down as Fig. 1(a) at $T=60$ mK; data in (b) were taken from another cool down after Fig. 1(b) at $T=60$ mK with unchanged G_N. The current of the smallest I_{CM} curve in (b) has been amplified by a factor of 5 for clarity. Black and red (light gray) solid lines in (c) are theoretical fits using Eq. (1).

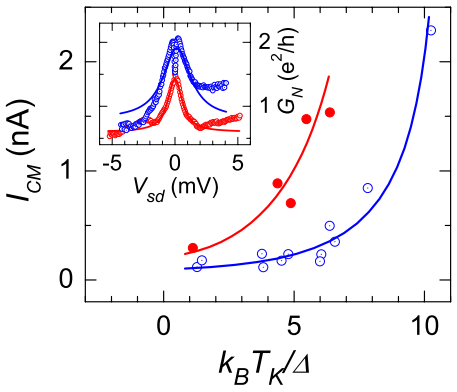

FIG. 3. (Color online) Measured critical current I_{CM} versus scaled Kondo energy k_BT_K/Δ for Kondo resonances marked by red (light gray) and blue (dark gray) arrows in Fig. 1. Peaks with zero-field splitting are denoted by blue circles, while red dots refer to nonsplit peaks in Fig. 1(b). The two solid curves are to guide the eyes. The inset shows two typical G_N-V_{ds} relations for the different kinds of conductance peaks and their Lorentzian fits. The curve for nonsplit peak has been shifted downwards by 0.3 units for clarity.

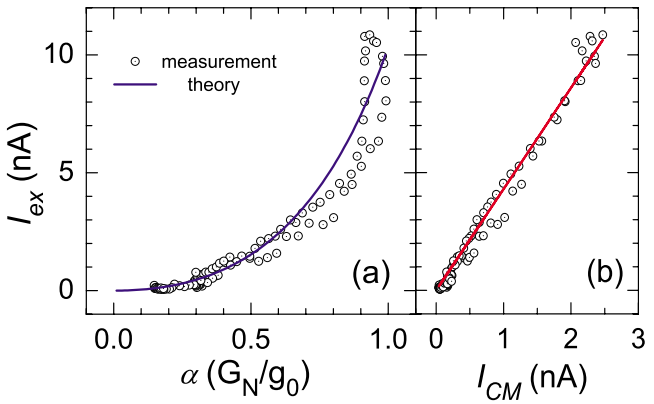

FIG. 4. (Color online) Excess current I_{ex} of one Kondo resonance with $T_K=14$ K at $T=90$ mK versus (a) transmission coefficient $\alpha=G_N/g_0=G_N/(2e^2/h)$ and (b) measured critical current I_{CM}. The blue (dark gray) line in (a) is the theoretical curve from Eq. (2) with $\tilde{\Delta}=100$ μeV and red (light gray) line in (b) gives linear fit of $I_{ex}/I_{CM}=4.3$

Fig. 2(c), with $I_{0M}=5.3$ and 3.3 nA corresponding to Fabry-Pérot and Kondo regimes, respectively (the latter at $T_K=14$ K).

As in the FP regime, the largest critical current over a Kondo resonance corresponds to the peak value of the normal-state conductance. In addition, the magnitude of I_{CM} depends on the width of the resonance in bias voltage, i.e., on T_K. We have fitted the conductance peaks $G_d(V_{ds})$ with a Lorentzian function in order to extract the Kondo temperature T_K. The resulting I_{CM}-T_K correlation is plotted in Fig. 3 which displays two branches, instead of a single-valued correlation as observed by Grove-Rasmussen *et al.*[16] The upper and lower branches involve the resonance peaks marked in Fig. 1 by red and blue arrows, respectively. Due to the problem of trapped charge fluctuating on the back gate, we have been forced to present only data on which we are sure of the identification between critical current and normal-state conductance. As shown in the inset of Fig. 3, in the data of the lower branch, there is a small dip on the zero-bias conductance peak signifying zero-field splitting of the Kondo resonances marked by blue arrows. The Lorentzian fitting on the split peaks is somewhat approximative, and the fitted T_K remains a bit smaller than from the true half width. Nevertheless, this uncertainty is insignificant on the scale of separation of the upper and lower branches in Fig. 3. Notice that $k_BT_K \sim E_C > \Delta \gg k_BT$ is valid for all of the measured resonance peaks, which indicates that the transport mechanism is dominated by Kondo effect and Coulomb blockade.

Zero-field splitting seems to take place in our data in every second Kondo resonance, as seen in the nearly alternating sequence of red and blue arrows in Fig. 1(b). Previously zero-field Kondo-peak splitting has been reported in Ref. 23, where the splitting originates from magnetic impurity, which is different from our case as the splitting should then be seen at all the Kondo resonances. Using the standard fourfold shell-filling sequence, it is hard to explain our findings. Split Kondo ridges may be observable when the dot is occupied by two electrons ($N=2$),[3,24] and the energy scale of the splitting equals to the gap between singlet ground state and triplet excited state. This, however, should be bordered from both sides by standard spin-half Kondo peaks, a sequence that we cannot identify in our data. From the normal-state bias maps, the characteristic zero-field splitting energy can be estimated as $\Delta_{ZBS} \sim 0.4$ meV, which is well above MAR peak of superconducting electrodes $2\Delta=0.25$ meV and the typical singlet-triplet excitation energy as found in Ref. 3. We conjecture that the observed zero-field splitting is related to the SU(4) Kondo effect which is peculiar to carbon nanotubes[25,26] and which has been shown to lead to a dip in the density of states at small energies,[27] which can also suppress the superconducting critical current. Alternatively, zero-field splitting may be related with the recent observation of non-negligible spin-orbit coupling in SWNTs[28] which can result in the large splitting energy we observed. In any case, SU(4) Kondo can explain the unusually high T_K by the enhanced degeneracy of a multiple-level quantum dot.[29]

According to theory,[30] the width of Andreev levels can be substantially renormalized by the Kondo effect, which would also modify the *IV* curve. In order to look for the gap renormalization, we have extracted the excess current I_{ex} as a function of normal-state transmission coefficient α, which is displayed in Fig. 4, with α calculated from $\alpha=G_N/(2e^2/h)$, and I_{ex} determined by the difference of integration from G_d-V_{ds} curves in superconducting/normal state like in Ref. 31. The relation between I_{ex} and α in a quantum point contact[32–34] can be written as $I_{ex}=I_{ex1}+I_{ex2}$, where

$$I_{ex1} = \frac{e\Delta_g}{h}\frac{\alpha^2}{(2-\alpha)\sqrt{1-\alpha}}\ln\left[\frac{1+[2\sqrt{1-\alpha}/(2-\alpha)]}{1-[2\sqrt{1-\alpha}/(2-\alpha)]}\right],$$

$$I_{ex2} = \frac{e\Delta_g}{h}\alpha^2\left[\frac{1}{1-\alpha}+\frac{2-\alpha}{2(1-\alpha)^{3/2}}\ln\left(\frac{1-\sqrt{1-\alpha}}{1+\sqrt{1-\alpha}}\right)\right]. \quad (2)$$

The blue curve in Fig. 4(a) illustrates Eq. (2) with $\Delta_g \equiv \tilde{\Delta}=100$ μeV, indicating a gap renormalization of $\tilde{\Delta}/\Delta=0.8$. We have also investigated the relation between I_{ex} and I_{CM} at

different gate voltages. The data are shown in Fig. 4(b), which yield a linear relation with $I_{ex}/I_{CM}=4.3$ at $T_K=14$ K; this arises because both are proportional to α^2. MAR-induced current at large bias voltage gives $I_{AR}=4e\Delta/h$.[35] By taking into account that $I_{0M}\sim\frac{1}{10}I_0$, we get $I_{AR}/I_{CM}\sim\frac{20}{\pi}$, which is close to the measured I_{ex}/I_{CM} value.

In summary, we have investigated experimentally the proximity-effect-induced supercurrents in SWNTs in the Kondo regime and compared them with results in the Fabry-Pérot regime with equivalent conductance. In the Kondo regime, two different types of resonances, either split or non-split at zero-bias, were observed and this behavior reflected also in the magnitude of supercurrent that displayed two branches vs T_K. The excess current in Kondo regime was analyzed using MAR theory and renormalization of Andreev levels by 80% was obtained.

We wish to acknowledge fruitful discussions with S. Andresen, J. C. Cuevas, T. Heikkilä, J. Voutilainen, A. D. Zaikin, K. Flensberg, G. Cuniberti, T. Kontos, L. Lechner, P.-E. Lindelof, C. Strunk, and P. Virtanen. This work was supported by the Academy of Finland and by the EU under Contract No. FP6-IST-021285-2.

*Present address: Institut für Nanotechnologie, Forschungszentrum Karlsruhe, 76021 Karlsruhe, Germany.

[1] D. Goldhaber-Gordon, H. Shtrikman, D. Mahalu, D. Abusch-Magder, U. Meirav, and M. A. Kastner, Nature (London) **391**, 156 (1998).
[2] S. M. Cronenwett, T. H. Oosterkamp, and L. P. Kouwenhoven, Science **281**, 540 (1998).
[3] J. Nygård, D. H. Cobden, and P. E. Lindelof, Nature (London) **408**, 342 (2000).
[4] M. R. Buitelaar, T. Nussbaumer, and C. Schönenberger, Phys. Rev. Lett. **89**, 256801 (2002).
[5] W. Liang, M. Bockrath, D. Bozovic, J. H. Hafner, M. Tinkham, and H. Park, Nature (London) **411**, 665 (2001).
[6] S. J. Tans, M. H. Devoret, H. Dai, A. Thess, R. E. Smalley, L. J. Geerligs, and C. Dekker, Nature (London) **386**, 474 (1997).
[7] A. Yu. Kasumov, R. Deblock, M. Kociak, B. Reulet, H. Bouchiat, I. I. Khodos, Yu. B. Gorbatov, V. T. Volkov, C. Journet, and M. Burghard Science **284**, 1508 (1999); A. Kasumov, M. Kociak, M. Ferrier, R. Deblock, S. Guéron, B. Reulet, I. Khodos, O. Stéphan, and H. Bouchiat, Phys. Rev. B **68**, 214521 (2003).
[8] A. F. Morpurgo, J. Kong, C. M. Marcus, and H. Dai, Science **286**, 263 (1999).
[9] P. Jarillo-Herrero, J. A. van Dam, and L. P. Kouwenhoven, Nature (London) **439**, 953 (2006).
[10] J.-P. Cleuziou, W. Wernsdorfer, V. Bouchiat, T. Ondarçuhu, and M. Monthioux, Nat. Nanotechnol. **1**, 53 (2006).
[11] H. I. Jørgensen, T. Novotný, K. Grove-Rasmussen, K. Flensberg, and P. E. Lindelof, Nano Lett. **7**, 2441 (2007).
[12] Y. Zhang, G. Liu, and C. N. Lau, Nanoscale Res. Lett. **1**, 145 (2008).
[13] T. Tsuneta, L. Lechner, and P. J. Hakonen, Phys. Rev. Lett. **98**, 087002 (2007).
[14] E. Pallecchi, M. Gaaß, D. A. Ryndyk, and Ch. Strunk, Appl. Phys. Lett. **93**, 072501 (2008).
[15] See, e.g., C. W. J. Beenakker and H. van Houten, in *Single-Electron Tunneling and Mesoscopic Devices*, edited by H. Koch and H. Lübbig (Springer, Berlin, 1992), pp. 175–179 (reprinted in arXiv:cond-mat/0111505).
[16] K. Grove-Rasmussen, H. I. Jørgensen, and P. E. Lindelof, New J. Phys. **9**, 124 (2007).
[17] F. Wu, P. Queipo, T. Tsuneta, T. H. Wang, E. Kauppinen, and P. J. Hakonen, Phys. Rev. Lett. **99**, 156803 (2007).
[18] J. A. van Dam, Y. V. Nazarov, E. P. A. M. Bakkers, S. De Franceschi, and L. P. Kouwenhoven, Nature (London) **442**, 667 (2006).
[19] Quantitive discussion on the slope of NDR has to include the competition of E_C and E_J together with MAR current of the Josephson junction. See, e.g., E. Vecino, M. R. Buitelaar, A. Martín-Rodero, C. Schönenberger, and A. Levy Yeyati, Solid State Commun. **131**, 625 (2004).
[20] This value does not include the effect of finite length of the nanotube, which would suppress the maximum I_0 a bit. See, e.g., A. V. Galaktionov and A. D. Zaikin, Phys. Rev. B **65**, 184507 (2002).
[21] G.-L. Ingold, H. Grabert, and U. Eberhardt, Phys. Rev. B **50**, 395 (1994).
[22] When NDR exists, we extract I_{CM} from the local current maximum I_{CM_p} and minimum I_{CM_n} using $I_{CM}=(I_{CM_p}-I_{CM_n})/2$. Around the Kondo resonance peaks without NDR, I_{CM} is obtained using the averaged voltages, $\overline{V_{CM_p}}$ and $\overline{V_{CM_n}}$, respectively, of the $\overline{I_{CM_p}}$ and $\overline{I_{CM_n}}$ peak positions at lower I_{CM}, and taking $I_{CM}=I(\overline{V_{CM_p}})-I(\overline{V_{CM_n}})/2$.
[23] J. Nygård, W. F. Koehl, N. Mason, L. DiCarlo, and C. M. Marcus, arXiv:cond-mat/0410467 (unpublished).
[24] B. Babić, T. Kontos, and C. Schönenberger, Phys. Rev. B **70**, 235419 (2004).
[25] P. Jarillo-Herrero, J. Kong, H. S. J. van der Zant, C. Dekker, L. P. Kouwenhoven, and S. De Franceschi, Nature (London) **434**, 484 (2005).
[26] A. Makarovski, A. Zhukov, J. Liu, and G. Finkelstein, Phys. Rev. B **75**, 241407(R) (2007).
[27] J. S. Lim, M.-S. Choi, M. Y. Choi, R. López, and R. Aguado, Phys. Rev. B **74**, 205119 (2006).
[28] F. Kuemmeth, S. Ilani, D. C. Ralph, and P. L. McEuen, Nature (London) **452**, 448 (2008).
[29] T. Inoshita, A. Shimizu, Y. Kuramoto, and H. Sakaki, Phys. Rev. B **48**, 14725 (1993).
[30] A. L. Yeyati, A. Martin-Rodero, and E. Vecino, Phys. Rev. Lett. **91**, 266802 (2003).
[31] H. I. Jørgensen, K. Grove-Rasmussen, T. Novotny, K. Flensbert, and P. E. Lindelof, Phys. Rev. Lett. **96**, 207003 (2006).
[32] D. Averin and A. Bardas, Phys. Rev. Lett. **75**, 1831 (1995).
[33] E. N. Bratus', V. S. Shumeiko, and G. Wendin, Phys. Rev. Lett. **74**, 2110 (1995).
[34] J. C. Cuevas, A. Martín-Rodero, and A. L. Yeyati, Phys. Rev. B **54**, 7366 (1996).
[35] Y. Avishai, A. Golub, and A. D. Zaikin, Phys. Rev. B **67**, 041301(R) (2003).